



## Journal of Advanced Research in Applied Mechanics

Journal homepage:  
[https://semarakilmu.com.my/journals/index.php/appl\\_mech/index](https://semarakilmu.com.my/journals/index.php/appl_mech/index)  
ISSN: 2289-7895



# Plasma Power Effect to the Structure and Morphology of Strontium Stannate Thin Film

Yusmar Palapa Wijaya<sup>1,5</sup>, Khairul Anuar Mohamad<sup>1,\*</sup>, Afishah Alias<sup>2</sup>, Zulkifli Azman<sup>1</sup>, Bablu Kumar Ghosh<sup>3</sup>, Abu Bakar Abd Rahman<sup>4</sup>

- <sup>1</sup> Faculty of Electrical and Electronics Engineering, Universiti Tun Hussein Onn, Parit Raja 86400 Batu Pahat, Johor, Malaysia  
<sup>2</sup> Faculty of Applied Science and Technology, Universiti Tun Hussein Onn Panchor, Pagoh, 84600 Muar, Johor, Malaysia  
<sup>3</sup> Faculty of Engineering, University Malaysia Sabah, 88400 Kota Kinabalu, Sabah, Malaysia  
<sup>4</sup> Faculty of Science and Natural Resources, University Malaysia Sabah, 88400 Kota Kinabalu, Sabah, Malaysia  
<sup>5</sup> Department of Electronics System Engineering Technology, Politeknik Caltex Riau, Kota Pekanbaru, Riau 28265, Indonesia

### ARTICLE INFO

#### Article history:

Received 29 September 2024  
Received in revised form 31 October 2024  
Accepted 6 November 2024  
Available online 30 November 2024

#### Keywords:

SrSnO<sub>3</sub>; RF magnetron sputtering; perovskite oxide; RF plasma power; W-H plot

### ABSTRACT

Hybrid p-n heterojunction requires a suitable n-type material to support the charge transfer process in photodiode or solar cell applications. Numerous materials have been researched in terms of wet and dry processes. This paper investigated the effect of varied plasma power levels of 50 W, 80 W and 100 W at room temperature on the structure and morphology of an alkaline-earth-based perovskite oxide thin film. Strontium stannate (SrSnO<sub>3</sub>) thin films are deposited on an indium tin oxide (ITO) substrate using radio frequency (RF) magnetron sputtering at various power levels. The crystallographic orientation of the thin films was examined and it was observed that the (102) plane exhibited dense growth at low power, while the (002) plane showed increased intensity at higher power levels. Additionally, the increase in RF power resulted in larger crystallite and grain sizes, along with modified grain boundaries. Contrarily, surface roughness, resistivity, macrostrain and work adhesion were reduced. The nearly zero W-H linear fitting plot observed at 80 W can serve as a valuable reference for the fabrication of preferred films. These findings provide valuable insights for optimising the growth conditions of alkaline-earth-based perovskite oxide thin films for various applications.

## 1. Introduction

Strontium stannate (SrSnO<sub>3</sub>) is a perovskite-structured semiconducting material with a direct wide band gap ranging from 3.9 eV to 4.2 eV, enabling it to efficiently absorb light in the ultraviolet region [1]. Strontium stannate has an orthorhombic structure and it belongs to Pbnm space group, with pseudo-cubic lattice constants of  $a = 5.709 \text{ \AA}$ ,  $b = 5.703 \text{ \AA}$  and  $c = 8.065 \text{ \AA}$  and it is classified as an n-type material [2]. However, this material suffers from lower mobility as compared with barium stannate (BaSnO<sub>3</sub>) perovskite [3]. Nevertheless, the literature suggests that structural modifications

\* Corresponding author.

E-mail address: [khairulam@uthm.edu.my](mailto:khairulam@uthm.edu.my)

<https://doi.org/10.37934/aram.127.1.163171>

on alkaline-earth (Ba, Sr, Ca) stannates have made them promising semiconducting materials for photodetector [4], solar cell [5] and photocatalysis [6] applications.

Strontium stannate has been synthesised using various wet-processes such as sol-gel [7], the hydrothermal method [8], the Pechini method [9], polymeric precursor method [10] and calcination [11]. In contrast, Wakana *et al.*, demonstrated the dry process synthesis of SrSnO<sub>3</sub> on a magnesium oxide (MgO) substrate using the sputtering technique [12]. This technique required a solid target material containing moulded SrSnO<sub>3</sub> powder. Plasma with the energetic inert gas argon collided with the target, resulting in the emission of SrSnO<sub>3</sub> atoms that were deposited on the substrate. The ionised inert gas argon was triggered by RF or DC power applied in the process. The sputtering power significantly influenced the density and distribution of the reactive species in the plasma, which in turn, affected the growth, nucleation and deposition rate of the thin film [13]. By controlling the power, deposition conditions, such as the film thickness, composition and surface roughness, can be optimised. For certain metal materials with high hardness, a significant amount of power, such as DC sputtering or HiPIMS add-ons, is required [14]. On the other hand, the use of RF power is preferred for softer materials, such as SrSnO<sub>3</sub>. Several single or composite materials have been investigated related to RF sputtering power's effects on material properties, including indium thin oxide (ITO) [15], silicon dioxide (SiO<sub>2</sub>) [16], aluminium gallium nitride (AlGaN) [17], zinc oxide (ZnO) [18], aluminium-doped ZnO (AZO) [19] and copper nitride (Cu<sub>3</sub>N) [20].

In this study, SrSnO<sub>3</sub> thin films were synthesised using the RF magnetron sputtering method with RF power ranging from 50 W to 100 W. The effects of different plasma power levels on the structure, surface morphology and electrical properties were examined. This paper investigated the behaviour of thin films in order to obtain a high-quality SrSnO<sub>3</sub> thin film. The results demonstrated that crystal structure characteristics can be controlled by adjusting the RF sputtering power.

## 2. Methodology

### 2.1 Fabrication

A glass-coated Indium Thin Oxide (In<sub>2</sub>O<sub>3</sub>:Sn) substrate, known as ITO of 2 × 2 cm<sup>2</sup> was prepared. The ITO/glass substrate was cleaned by placing it in an ultrasonic bath containing acetone, methanol and de-ionised water. After the cleaning process, the substrate was dried in the oven for 10 minutes at 70° C. This process was important to ensure the substrate's surface is clean from any impurities that may affect its contact quality.

In the experiment, a RF power source with varying outputs of 50 W, 80 W and 100 W at a frequency of 13.65 MHz was utilised for the deposition process. Power was limited to 100 W due to target arcing at high power level. The chamber was maintained at a base pressure of 8.5 × 10<sup>-6</sup> Torr and a working pressure of 5 mTorr. During the process, the substrate was rotated at a speed of 5 rpm per hour per sample, positioned 120 mm away from the target and set at a non-perpendicular height. A mixture of pure inert sputter gas (75% Argon) and reactive gas (25% O<sub>2</sub>) was used, while the target material was a 99.9% pure SrSnO<sub>3</sub>-depleted compound sourced from Plasmaterials Co and measured 3 inches in diameter and 0.125 inches in thickness. A single cathode, set at an angle of 45 degrees to the base and with a bias voltage of 0 V, was connected to the RF power source. To improve the efficiency of the sputtering process for depositing three substrates under different parameters, an isolation gate valve (load lock) was employed to switch the substrates.

The addition of oxygen aimed to improve the deposition of thin film by reducing oxygen vacancies. Inert gas would bombard and collide with the target atoms, freeing them into the plasma. As a result, SrSnO<sub>3</sub> atoms would move kinetically towards the substrate and form a thin film. The sputtering system has numerous components and a chamber and its ambiance is controlled by a

turbo molecular pump (TMP) while being monitored by a vacuum gauge to achieve a high vacuum condition for establishing plasma. This system is fully controlled and monitored by a programmable logic controller (PLC) with a LabVIEW graphical user interface (GUI).

## 2.2 Characterization

The SrSnO<sub>3</sub> films were characterised via X-Ray diffraction (XRD) (PANalytical X'Pert Pro XRD System) by employing Cu-K $\alpha$  radiation at  $\lambda=0.152$  nm. A Hitachi 5100N atomic force microscope (AFM) was used for surface morphology observation, while electrical properties were analysed using a four-point probe to obtain optical characteristics. Surface tension was observed using the VCA Optima XE Contact Angle Goniometer (AST Products Inc).

## 3. Results and Discussion

The XRD patterns for SrSnO<sub>3</sub> thin films deposited at different RF power levels are depicted in Figure 1. At low RF power of 50 W, there was a single peak at  $2\theta = 35.5^\circ$  corresponding to the (102) plane. At higher power levels (80 W and 100 W), increased ion energy and density of the inert gas argon led to deeper penetration into the SrSnO<sub>3</sub> target, resulting in a considerable particle dispersion. The preferred orientations of SrSnO<sub>3</sub> crystal peaks appeared at (020), (002), (102), (031), (220), (040), (311) and (133) planes. It should be noted that at 50 W, the (102) plane showed a higher intensity compared with that of the (002) plane. Generally, in order to achieve a homogeneous substrate surface, a low RF power could be used with a longer deposition. However, in this case, at higher RF power levels, the (002) plane was more dominant than (102) plane in terms of intensity. As shown in Table 1, the intensity of (002) plane at 80 W and 100 W evidenced a progressive growth.

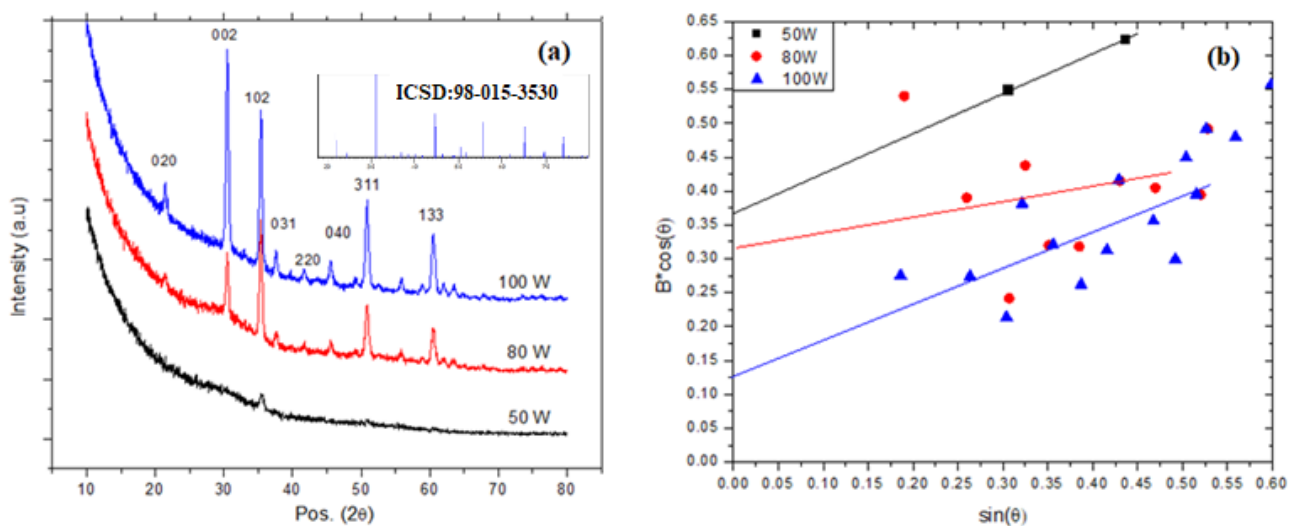


**Fig. 1.** Deposition of SrSnO<sub>3</sub> at 50 W, 80 W and 100 W (a) XRD patterns (b) Williamson-Hall (W-H) plot

Figure 1(b) depicts the data extraction from the XRD patterns shown in Figure 1(a), for obtaining the average strain and average crystallite size. To determine both parameters, a Williamson-Hall plot was used, which is expressed by the following equation:

$$\beta_{total} \cos \theta = C_{\epsilon} \sin \theta + \frac{k\lambda}{D_{W-H}} \quad (1)$$

where  $\beta_{total}$  is the total full width at half maximum (FWHM) of different peaks,  $\lambda$  is the X-ray wavelength (Cu –  $K\alpha = 1.5418 \text{ \AA}$ ),  $k = 0.94$  is the shape factor,  $C_\epsilon$  is the average strain,  $D_{W-H}$  is the crystal size and  $2\theta$  is the peak position. This equation can define the slope ( $m = C_\epsilon$ ) and intercept ( $C = K\lambda / D_{W-H}$ ), as expressed by the linear equation,  $y = mx + C$ . As shown in Figure 1(b), all the positive slope trends indicate that all thin films experienced tensile strain instead of compressive strain. At the low power of 50 W, the thin film exhibited an average crystallite size was 241.5 Å which was the smallest compared with the crystallite sizes of thin films deposited at the higher power levels, which were 275 Å at 80 W and 708 Å at 100 W. This indicates that the low kinetic energy yielded by the low RF sputtering power at 50 W did not have a significant impact on crystallite size. At 50 W, the strain was 0.266% by measuring  $C_\epsilon$ , indicating that low RF power had insufficient kinetic energy to overcome the surface energy barrier of the substrate. As power increased to 80 W, the film experienced a reduction in strain to 0.1%. However, at 100 W, the strain increased to 0.24%, possibly affected by the increasing density of atoms deposited.

Table 1 shows atomic condition information at peak positions  $2\theta = 30.45^\circ$  and  $2\theta = 35.5^\circ$ . The d-spacings of these planes were relatively stable, around 2.92 Å and 2.53 Å for (002) and (102) planes, respectively. When the RF power increased, the atoms had more kinetic energy to overcome the surface energy barrier of the substrate, which promotes larger crystallite size. The microstrain surrounding the crystals also decreased with increased RF power. Generally, an increased crystallite size can improve thermal and mechanical stability. However, larger crystallite sizes can increase brittleness and reduce ductility [21].

**Table 1**

XRD data of (002) and (102) peaks

| Sputtering power (watt) | $2\theta$ pos. | (hkl) | $\Delta$ Intensity* (a.u) | FWHM  | d-spacing (Å) | Crystallite Size (Å) | Micro strain (%) |
|-------------------------|----------------|-------|---------------------------|-------|---------------|----------------------|------------------|
| 50                      | $30.41^\circ$  | (002) | N/A                       | N/A   | N/A           | N/A                  | N/A              |
|                         | $35.5^\circ$   | (102) | 98                        | 0.59  | 2.52          | 160.18               | 0.78             |
| 80                      | $30.45^\circ$  | (002) | 488                       | 0.413 | 2.92          | 227.30               | 0.64             |
|                         | $35.34^\circ$  | (102) | 983                       | 0.26  | 2.53          | 364.33               | 0.34             |
| 100                     | $30.53^\circ$  | (002) | 1641                      | 0.29  | 2.92          | 322.04               | 0.45             |
|                         | $35.34^\circ$  | (102) | 1270                      | 0.23  | 2.53          | 413.26               | 0.30             |

\*: intensity peak subtracted by baseline

Figure 2 below depicts the surface images scanned via AFM.

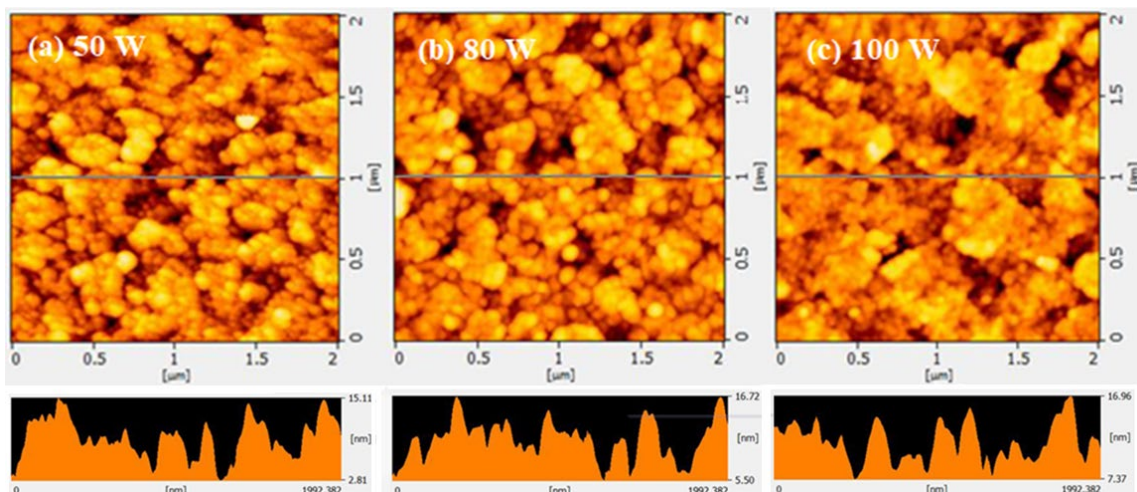


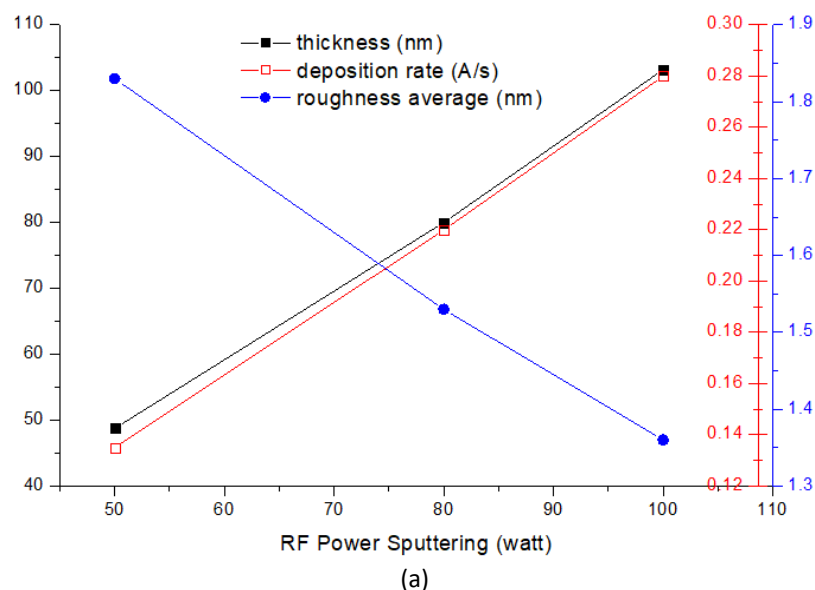
**Fig. 2.** Atomic force microscopy (AFM) topography images (a) 50 W (b) 80 W (c) 100W

Surface characteristics were observed via AFM using a touching cantilever to scan a  $4 \mu\text{m}^2$  area. Figure 2(a) to Figure(c) depicts the surface of the films to reveal the atomic arrangement on the substrate. It should be noted that surface roughness depends on the applied RF power in the deposition process. A larger crystallite size and decreased roughness in accumulation can affect the grain size, providing the benefits of higher film conductivity or lower resistivity, as shown in Figure 3(b) [22]. High-energy ions, were generated by RF power, can also increase the surface mobility of atoms on a substrate's surface, resulting in more efficient migration and rearrangement of atoms, promoting larger and more ordered crystal structures. Vopsaroiu *et al.*, [23] revealed that RF sputtering power can control grain size for a chromium (Cr) target, where a higher power yielded larger grains. In AFM, the roughness root mean square (RMS) can be defined as  $S_q$  and is expressed as:

$$S_q = \sqrt{\frac{1}{n} \sum_{i=1}^n y_i^2} \quad (2)$$

where  $n$  is the maximum number of points scanned and  $y_i$  is the surface height at a certain point. Roughness trended lower as RF sputtering power increased, as seen in Figure 3(a). The thin films' roughness was affected by the boundaries between grains. This indicates that the higher the number of grains, the more boundaries there were, which in turn increased the scattering. There are plenty of factors that contribute to surface roughness, such as surface texture, topography and the presence of defects or impurities. Thus, grain boundary is not the only factor that contributes to surface roughness.

From Figure 3(a), it can be noted that thickness increased from 50 to 100 nm and the deposition rate increased from 0.14 to 0.28 Å/s as RF power increased. Physically, increased power can emit more atoms from a target due to a higher kinetic energy. The excessive amounts of atoms bombard the substrate immediately in the plasma's atmosphere. This behaviour has also been revealed in several materials, such as ITO, ZnO and  $\text{Cu}_3\text{N}$ , due to the effect of RF sputtering power. Figure 3(b) shows RF sputtering power against resistivity and grain size. As shown in Figure 3(b), the grain sizes of films are 159.3 nm, 188.4 nm and 198.3 nm for 50 W, 80 W and 100 W, respectively. At higher RF power levels, the grain size increased while resistivity decreased, in the thin films.



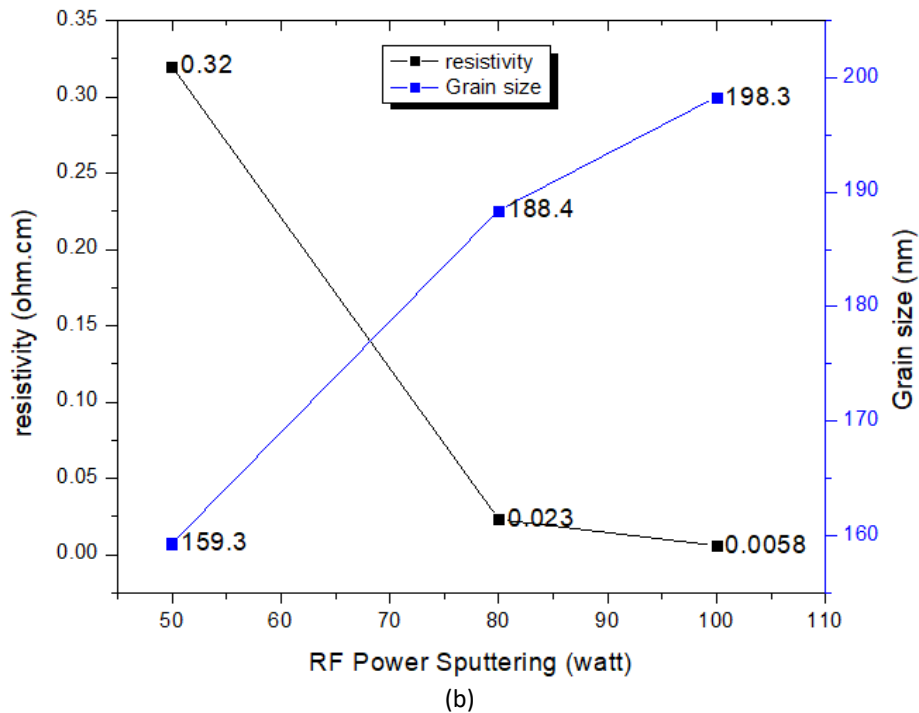


**Fig. 3.** (a) Plot of thickness, deposition rate and average roughness average versus RF sputtering power (b) resistivity and grain comparison

Figure 4 shows the hydrophobicity of surface characteristics measured using a goniometer. When a droplet of liquid is placed on a flat surface, the balance of the three-phase interface is expressed by Young's equation, as follows:

$$\gamma_s = \gamma_{sl} + \gamma_l \times \cos \theta \quad (3)$$

where  $\gamma_l$  is the surface tension of the liquid,  $\gamma_{sl}$  is the interfacial tension,  $\gamma_s$  is the surface energy of the solid and  $\theta$  is the contact angle between the liquid-air interface and the surface [24]. The thin films showed contact angles of  $50.2^\circ$ ,  $56.0^\circ$  and  $64.8^\circ$  when deposited at 50 W, 80 W and 100 W power levels, respectively. This indicates that all deposited films were hydrophilic. Work of adhesion or surface energy, can be determined via contact angle using the following equation:

$$W_a = g_{LV}(1 + \cos \theta) \quad (4)$$

where  $W_a$  is the work of adhesion,  $g_{LV}$  is the surface tension of water in the air (73 dyne/cm) and  $\theta$  is the contact angle. The surface energy values of the thin film deposited at 50 W, 80 W and 100 W were 119.72 dyne/cm, 113.82 dyne/cm and 104.08 dyne/cm, respectively.

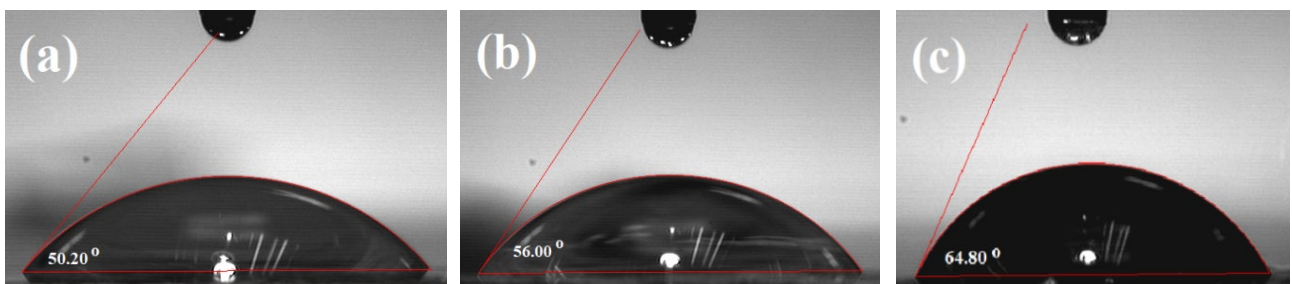


**Fig. 4.** Contact angle of films at (a)50 W (b) 80 W (c) 100 W

Many researchers have reported a direct proportional relationship between surface roughness and contact angle, signifying that an increase in roughness leads to an increase in contact angle [25]. This correlation is supported by the Wenzel model, which concludes that surface roughness amplifies wettability on the original surface. However, as depicted in Figure 4, the increase in RF power weakened the work of adhesion of SrSnO<sub>3</sub> films to the substrate. This behaviour depended on the characteristics of the material.

#### 4. Conclusions

This paper presents a successful demonstration of SrSnO<sub>3</sub> thin film deposition using RF magnetron sputtering. The effect of varying RF power levels was investigated on the structure, morphology and electrical behaviour of the SrSnO<sub>3</sub> thin film. At a low RF power level of 50 W, the (102) plane exhibited a more substantial growth (98 a.u.) compared with those of other planes, indicating a lower surface barrier energy for its formation. However, the (002) plane grew progressively at the medium power (488 a.u.) and high power (1641 a.u.) due to the higher kinetic energy on the surface, whereas the (102) plane weakened at 100 W of RF power. The increase in RF sputtering power influenced crystal size (241.5 Å to 708 Å), which was related to grain size and grain boundary. Contrarily, it caused decreased surface roughness, resistivity and macrostrain. Based on Williamson-Hall analysis, it was furthermore found that the SrSnO<sub>3</sub> film exhibited tensile strain, as indicated by gradient values. The increasing RF sputtering power resulted in weakened work of adhesion or surface energy of the thin films (119.72 dyne/cm to 104.08 dyne/cm), which indicated that, at increased power, less energy was required to separate the thin film from the substrate. Based on this study, the increase in sputtering power can enhance the ion density in a plasma, which in turn leads to higher ion bombardment energy on a substrate. Thus, this promotes the nucleation of crystals and the growth of larger crystals. The nearly zero W-H linear fitting at 80 W can be optionally used as a reference to fabricate preferred films.

#### Acknowledgement

This work is supported by the Ministry of Higher Education Malaysia under the Fundamental Research Grant Scheme (FRGS/1/2018/TK10/UTHM/03/7). The author would like to thank Microelectronic and Nanotechnology-Shamsuddin Research Centre (MiNT-SRC), Universiti Tun Hussein Onn Malaysia for providing excellent laboratory facilities. Additionally, special thanks are extended to Faezahana Mokhter and Azwadi Umar for their valuable assistance.

#### References

- [1] Riza, Muhammad Arif, Suhaila Sepeai, Norasikin Ahmad Ludin, Mohd Asri Mat Teridi and Mohd Adib Ibrahim. "Synthesis and Characterization of SrSnO<sub>3</sub> Using Different Synthesis Methods." *Malaysian J. Anal. Sci* 23, no. 1 (2019): 100-108.
- [2] Abd Rahman, A. B., M. S. Sarjadi, A. Alias and M. A. Ibrahim. "Fabrication of stannate perovskite structure as optoelectronics material: An overview." In *Journal of Physics: Conference Series*, vol. 1358, no. 1, p. 012043. IOP Publishing, 2019. <https://doi.org/10.1088/1742-6596/1358/1/012043>
- [3] Ong, Khuong P., Xiaofeng Fan, Alaska Subedi, Michael B. Sullivan and David J. Singh. "Transparent conducting properties of SrSnO<sub>3</sub> and ZnSnO<sub>3</sub>." *APL Materials* 3, no. 6 (2015). <https://doi.org/10.1063/1.4919564>
- [4] Kim, Hoon Min, Useong Kim, Chulkwon Park, Hyukwoo Kwon and Kookrin Char. "Thermally stable pn-junctions based on a single transparent perovskite semiconductor BaSnO<sub>3</sub>." *Appl Materials* 4, no. 5 (2016). <https://doi.org/10.1063/1.4952609>
- [5] Shin, Seong Sik, Eun Joo Yeom, Woon Seok Yang, Seyoon Hur, Min Gyu Kim, Jino Im, Jangwon Seo, Jun Hong Noh and Sang Il Seok. "Colloidally prepared La-doped BaSnO<sub>3</sub> electrodes for efficient, photostable perovskite solar cells." *Science* 356, no. 6334 (2017): 167-171. <https://doi.org/10.1126/science.aam6620>

- [6] Honorio, L. M. C., M. V. B. Santos, EC da Silva Filho, J. A. Osajima, A. S. Maia and IMG dos Santos. "Alkaline earth stannates applied in photocatalysis: prospection and review of literature." *Cerâmica* 64, no. 372 (2018): 559-569. <https://doi.org/10.1590/0366-69132018643722480>
- [7] Gul, E. andrius Stanulis, Y. Barushka, Edita Garskaite, Rimantas Ramanauskas, Ayşe Uztetik Morkan and A. Kareiva. "The influence of thermal processing on microstructure of sol–gel-derived SrSnO<sub>3</sub> thin films." *Journal of Materials Science* 52 (2017): 12624-12634. <https://doi.org/10.1007/s10853-017-1385-y>
- [8] Bhat, Aadil Ahmad, M. Burhanuz Zaman, Javied Hamid Malik, Khurshaid Ahmad Malik, Insaaf Assadullah and Radha Tomar. "Facile way of making hydrothermally synthesized crystalline SrSnO<sub>3</sub> perovskite nanorods suitable for blue LEDs and spintronic applications." *ACS omega* 6, no. 25 (2021): 16356-16363. <https://doi.org/10.1021/acsomega.1c00831>
- [9] Teixeira, Ana Rita Ferreira Alves, Alex de Meireles Neris, Elson Longo, José Rodrigues de Carvalho Filho, Amer Hakki, Donald Macphee and Ieda Maria Garcia dos Santos. "SrSnO<sub>3</sub> perovskite obtained by the modified Pechini method—insights about its photocatalytic activity." *Journal of Photochemistry and Photobiology A: Chemistry* 369 (2019): 181-188. <https://doi.org/10.1016/j.jphotochem.2018.10.028>
- [10] Alves, Mary CF, Soraia C. Souza, Márcia RS Silva, Elaine C. Paris, S. J. G. Lima, R. M. Gomes, Elson Longo, A. G. De Souza and Iêda M. Garcia dos Santos. "Thermal analysis applied in the crystallization study of SrSnO<sub>3</sub>." *Journal of thermal analysis and calorimetry* 97 (2009): 179-183. <https://doi.org/10.1007/s10973-009-0242-x>
- [11] Bohnemann, Jörg, Rafael Libanori, Mário L. Moreira and Elson Longo. "High-efficient microwave synthesis and characterisation of SrSnO<sub>3</sub>." *Chemical Engineering Journal* 155, no. 3 (2009): 905-909. <https://doi.org/10.1016/j.cej.2009.09.004>
- [12] Wakana, H., Ai Kamitani, S. Adachi, K. Nakayama, Y. Ishimaru, Y. Tarutani and K. Tanabe. "Examination of deposition conditions for SrSnO<sub>3</sub> insulating layer for single flux quantum circuits." *Physica C: Superconductivity and its applications* 426 (2005): 1495-1501. <https://doi.org/10.1016/j.physc.2005.01.074>
- [13] Abdulrahman, Ahmed F., Azeez A. Barzinjy, Samir M. Hamad and Munirah Abdullah Almessiere. "Impact of radio frequency plasma power on the structure, crystallinity, dislocation density and the energy band gap of ZnO nanostructure." *ACS omega* 6, no. 47 (2021): 31605-31614. <https://doi.org/10.1021/acsomega.1c04105>
- [14] Loch, Daniel AL and Arutiun P. Ehiasarian. "Study of the effect of RF-power and process pressure on the morphology of copper and titanium sputtered by ICIS." *Surface and coatings technology* 327 (2017): 200-206. <https://doi.org/10.1016/j.surfcoat.2016.10.018>
- [15] Boussoum, O., M. S. Belkaid, Charles Renard, G. Halais and F. Farhati. "Effect of the annealing gas and RF power sputtering in the electrical, structural and optical properties of ITO thin films." *Journal of nano-and electronic physics* 11, no. 2 (2019): 02010-1. [https://doi.org/10.21272/jnep.11\(2\).02010](https://doi.org/10.21272/jnep.11(2).02010)
- [16] Zhao, Changjiang, Leran Zhao, Juncheng Liu, Zhigang Liu and Yan Chen. "Effect of sputtering power on the properties of SiO<sub>2</sub> films grown by radio frequency magnetron sputtering at room temperature." *Optical and Quantum Electronics* 53 (2021): 1-12. <https://doi.org/10.1007/s11082-020-02639-4>
- [17] Othman, Nur Afiqah, Nafarizal Nayan, Mohd Kamarulzaki Mustafa, Zulkifli Azman, Megat Muhammad Ikhsan Megat Hasnan, Siti Noryasmin Jaafar, Anis Suhaili Bakri *et al.*, "Effects of radio-frequency power on structural properties and morphology of AlGa<sub>N</sub> thin film prepared by co-sputtering technique." *ELEKTRIKA-Journal of Electrical Engineering* 20, no. 2 (2021): 14-18. <https://doi.org/10.11113/elektrika.v20n2.270>
- [18] Gao, Wei and Zhengwei Li. "ZnO thin films produced by magnetron sputtering." *Ceramics International* 30, no. 7 (2004): 1155-1159. <https://doi.org/10.1016/j.ceramint.2003.12.197>
- [19] Challali, Fatiha, Djelloul Mendil, Tahar Touam, Thierry Chauveau, Valérie Bockelée, Alexis Garcia Sanchez, Azeddine Chelouche and Marie-Paule Besland. "Effect of RF sputtering power and vacuum annealing on the properties of AZO thin films prepared from ceramic target in confocal configuration." *Materials Science in Semiconductor Processing* 118 (2020): 105217. <https://doi.org/10.1016/j.mssp.2020.105217>
- [20] Rodríguez-Tapiador, María Isabel, Jesús Merino, Tariq Jawhari, Ana Luz Muñoz-Rosas, Joan Bertomeu and Susana Fernández. "Power effect on the properties of copper nitride films as solar absorber deposited in pure nitrogen atmosphere." *Applied Research* 3, no. 1 (2024): e202200105. <https://doi.org/10.1002/appl.202200105>
- [21] Diao, Xin-Feng, Yan-lin Tang, Tian-yu Tang, Quan Xie, Kun Xiang and Gao-fu Liu. "Study on the stability of organic–inorganic perovskite solar cell materials based on first principle." *Molecular Physics* 118, no. 8 (2020): e1665200. <https://doi.org/10.1080/00268976.2019.1665200>
- [22] Ahmed, Naser M., Fayroz A. Sabah, H. I. Abdulgafour, Ahmed Alsadig, A. Sulieman and M. Alkhoaryef. "The effect of post annealing temperature on grain size of indium-tin-oxide for optical and electrical properties improvement." *Results in Physics* 13 (2019): 102159. <https://doi.org/10.1016/j.rinp.2019.102159>
- [23] Vopsaroiu, Marian, M. J. Thwaites, S. Rand, P. J. Grundy and K. O'grady. "Novel sputtering technology for grain-size control." *IEEE transactions on magnetics* 40, no. 4 (2004): 2443-2445. <https://doi.org/10.1109/TMAG.2004.828971>

- [24] Wiatrowski, Artur, Agata Obstarczyk, Michał Mazur, Danuta Kaczmarek and Damian Wojcieszak. "Characterization of HfO<sub>2</sub> optical coatings deposited by MF magnetron sputtering." *Coatings* 9, no. 2 (2019): 106. <https://doi.org/10.3390/coatings9020106>
- [25] Dave, Pranav Y., Kartik H. Patel, Kamlesh V. Chauhan, Amit Kumar Chawla and Sushant K. Rawal. "Examination of zinc oxide films prepared by magnetron sputtering." *Procedia Technology* 23 (2016): 328-335. <https://doi.org/10.1016/j.protcy.2016.03.034>